

The role of the screening potential in the deuteron-deuteron thermonuclear reaction rates

Faisal Etminan*

*Department of Physics, Faculty of Sciences,
University of Birjand, Birjand 97175-615, Iran*

(Dated: June 3, 2025)

The deuteron-deuteron (D-D) thermonuclear reaction rates in metallic environments (considering the electron screening effects) is calculated using the S-factor functions which were obtained by fitting to low-energy data on D-D reactions. For this purpose, a fitted S-factor model based on the NACRE compilation is employed. This limited the energy range of Big Bang nucleosynthesis (BBN) for the $^2\text{H}(d, p)^3\text{H}$ and $^2\text{H}(d, n)^3\text{He}$ reactions. The corresponding Maxwellian-averaged thermonuclear reaction rates of relevance in astrophysical plasmas at temperatures in the range from 10^6 K to 10^{10} (or 1.3×10^8) K are provided in tabular formats. In these evaluations, the screening energy (U_e) is assumed to be 100, 400, 750, 1000 eV and 1250 eV. This series of values has been selected based on theoretical and experimental studies conducted so far. Eventually, our numerical analysis suggests that the ratio of the reaction rate with the screening potential to the reaction rate without the screening potential, can be described by the term $\exp(4.70 + 6.50 U_e/T_9)$ for both $^2\text{H}(d, p)^3\text{H}$ and $^2\text{H}(d, n)^3\text{He}$ reactions.

I. INTRODUCTION

In astrophysical environments and present fusion experiments, nuclear reactions occur in the presence of other charges that impact the rates at which nuclear reactions occur. Therefore, it is important to know the fusion cross-sections and Maxwellian reactivities as precisely as possible for interpreting fusion rate measurements and predicting the fusion performance of future devices [1, 2]. Because of unique conditions of temperature, pressure,

* fetminan@birjand.ac.ir

and density in a stellar environment, the atoms can be ionized entirely to form a plasma, which is made of different nuclei and electrons. Moreover, the Coulomb interaction screening in plasma environments is a collective effect of correlated many-particle interactions. The ranges of densities (n) and temperatures (T) in dense astrophysical and laboratory plasmas are as follows, $n \sim 10^{15} - 10^{18} \text{ cm}^{-3}$, $T \sim 5.8 \times 10^3 - 5.8 \times 10^3 \text{ K}$ for stellar atmospheres, $n \sim 10^{19} - 10^{21} \text{ cm}^{-3}$, $T \sim 5.8 \times 10^5 - 3.5 \times 10^6 \text{ K}$ for laser-produced plasmas and $n \sim 10^{22} - 10^{26} \text{ cm}^{-3}$, $T \sim 5.8 \times 10^6 - 1.1 \times 10^8 \text{ K}$ for inertial confinement fusion plasmas.

Generally, in a plasma environment, there is a struggle between Coulomb potential and thermal (kinetic) energy, thus quantity Γ , known as the Coulomb coupling parameter, can be defined in a classical hot, dense plasma as [3, 4]

$$\Gamma = \frac{Z_1 Z_2 e^2}{R_i k_B T}, \quad (1)$$

where Z_i is the charge of ions in the plasma, $R_i = (3/4\pi n)^{1/3}$ the average inter-ionic distance, k_B the Boltzmann constant, T and n are the plasma electron temperature and density, respectively. At high temperatures and/or low densities (weakly coupled plasmas), when the thermal effects dominate over the Coulomb ones (like during stellar hydrostatic burning), $\Gamma \ll 1$, the charge screening effects is week, while at low temperatures and high densities (strongly-coupled plasmas), the Coulomb effects are dominant (such as in the solid phase, dense and relatively cold astrophysical plasma like giant planets, dwarfs, and type Ia supernova [2], $\Gamma \gg 1$, the charge screening effects are strong. If the most effective energy for nuclear reactions (E_0 in Eq.(5) also known as Gamow peak energy) is adequately larger than the thermal energy, the density fluctuations could activate the fusion reactions even at $T = 0 \text{ K}$ [5].

At astrophysical energies, far below the Coulomb barrier, the electron screening effect could describe the exponential-like enhancement of the nuclear fusion cross-sections measured in the atomic environment relative to the bare nuclei medium. First time, this enhancement was observed in the ${}^2\text{H}(d, p){}^3\text{H}$ and ${}^2\text{H}(d, n){}^3\text{He}$ reactions [6] and afterwards confirmed by several experiments [7–10] with deuteron beams and deuterated targets [11–13].

Actually, under terrestrial conditions, the D-D reactions in a metallic environments can be an ideal tool, since the S factor of this reaction is relatively significant, and the presence of quasi-free conduction and shell electrons of the metal lattice could leads to significant enhancement of the reaction yields [14, 15].

However, can it practically provide the thermonuclear fusion conditions on earth that would take advantage of this electron screening effect? If the answer is yes, what is the real contribution of this effect to the reaction rates? To answer these questions, let us look at recent achievements in this field. Quick and powerful compression can force materials to change their properties dramatically. Knudson et al. [16] succeeded in turning liquid deuterium into metal under extreme temperatures and pressures. And later, for the first time, Zaghou and co-authors [17] have found a method to transform a liquid metallic deuterium into a dense plasma and to recognize the temperature where a liquid under high-density conditions crosses over to a plasma state. Their observations have connection for improved understanding stars and could help in the realization of controlled thermonuclear fusion. Indeed, increasing the density to extreme conditions ($\rho_d = 0.774 \text{ g/cm}^3$) provided the liquid enters a state where it exhibited quantum properties; e.g., in a dense liquid metal, only two electrons can share the same state; nevertheless, when the temperature is increased to 0.4 Fermi temperature or 50,000 degrees Celsius ($T_F = 13.8 \text{ eV}$), the electrons rearrange themselves in a random process that simulates a hot soup of plasma, and the electrons detach their quantum nature and behave classically [17]. Unlike all other metals, fluid metallic deuterium has no bound electrons, and at sufficiently high density, it constitutes the archetypal one-component Coulomb system, where the ions are weakly coupled to the nearly free conduction electrons [17, 18].

Thus, the metallic deuterium targets could provide an excellent model (or small laboratory) for strongly coupled plasmas. The theoretical and experimental study of nuclear reaction rates in metallic environments have great importance for nuclear astrophysics [15, 19] like brown dwarfs and also represent the states of matter needed to achieve thermonuclear fusion [17]. According to the above discussion, we re-evaluate the D-D Maxwellian-averaged thermonuclear reaction rates by considering the screening effects to simulate the metallic deuterium plasma environment. Recently, Coc et al. [20] reevaluated the $^2\text{H}(p, \gamma)^3\text{He}$, $^2\text{H}(d, p)^3\text{H}$, and $^2\text{H}(d, n)^3\text{He}$ reaction rates that govern deuterium destruction, incorporating new experimental data and carefully accounting for systematic uncertainties. Contrary to previous evaluations [21–23] and measurements [24, 25], they used theoretical *ab initio* models for the energy dependence of the S factors. As a result, their rates increase at BBN temperatures, leading to a reduced value of $\text{D/H} = (2.45 \pm 0.10) \times 10^{-5} (2\sigma)$, in agreement with observations.

Although Ref. [25] provides the most up-to-date calculations for the reaction rate, in my calculation, I employed a fitted S-factor model based on the NACRE compilation [5] because the fitted functions in Ref. [5] used relatively more experimental data and based on the comparison made in Ref. [25], their measurement are in good agreement with the NACRE compilation. The NACRE compilation is limited to the energy range of BBN for the ${}^2\text{H}(d, p){}^3\text{H}$ and ${}^2\text{H}(d, n){}^3\text{He}$ reactions.

Finally, our numerical results of the reaction rates with and without the screening effects are given in a tabular way as a function of temperature. And, the dependence of the reaction rate on the screening potential, U_e is investigated by calculating the ratio of the reaction rate with the screening potential to the reaction rate without the screening potential as function of $U_e / (k_B T)$, and the results are fitted by an analytical function. These calculation could help in understanding of how to design experiments better to achieve fusion.

This paper is structured as follows: Sec. II, describes the formalism that has been adopted in order to derive the astrophysical rates of the charged particle-induced reactions. In addition to the general formulae used for the calculation of the Maxwellian-averaged reaction rates, it contains a description of the screened nuclear reaction cross-section, the non-resonant NACRE model of the data which is obtained by extrapolating to astrophysical energies. The numerical results are given in Sec. III, also the relevant discussions about the results are presented there. I summarize and conclude my work in Sec. IV.

II. GENERAL FORMALISM

A. Maxwellian-averaged reaction rates $N_A \langle \sigma v \rangle$

For two-body reactions with the relative velocity v and the cross section σ , the Maxwellian-averaged reaction rates (or Maxwellian-averaged reactivity) $N_A \langle \sigma v \rangle$ are defined as [26]

$$N_A \langle \sigma v \rangle = N_A \frac{(8/\pi)^{1/2}}{\mu^{1/2} (k_B T)^{3/2}} \int_0^\infty \sigma(E) E \exp\left(-\frac{E}{k_B T}\right) dE, \quad (2)$$

where N_A is the Avogadro number, μ the reduced mass of the system, and E the energy in the CM (center-of-mass) reference frame. When $N_A \langle \sigma v \rangle$ is indicating in $\text{cm}^3 \text{mol}^{-1} \text{s}^{-1}$, the energies E and $k_B T$ in MeV, and the cross-section σ in barn, Eq. (2) becomes

$$N_A \langle \sigma v \rangle = 3.7313 \times 10^{10} A^{-1/2} T_9^{-3/2} \int_0^\infty \sigma(E) E \exp(-11.605 E/T_9) dE, \quad (3)$$

where A is the reduced mass in amu, and T_9 is the temperature in units of 10^9 K. The numerical calculation of the rates is done from $T_9 = 0.001$ to $T_9 = 10$.

For nuclear fusion reactions that occur at thermal energies E well below the Coulomb barrier between interacting nuclei, the nuclear fusion cross-section of bare nucleus σ_{bare} usually can be written as [27]

$$\sigma_{\text{bare}}(E) = \frac{S(E)}{E} \exp(-2\pi\eta), \quad (4)$$

where $S(E)$ is known as the astrophysical S -factor which accounts for nuclear effects and is a function usually mildly varying with energy. Also, it factors out from $\sigma(E)$ the energy dependence of the de Broglie wavelength and the Coulomb penetrability. The quantity $\eta = Z_1 Z_2 e^2 / \hbar v = 0.1575 Z_1 Z_2 \left(\sqrt{A/E} \right)$ is the Sommerfeld parameter, Z_1 (Z_2) the charge numbers of the interacting nuclei, and \hbar the reduced Planck constant. The above formulas are not revised for screening by the electrons bound to the molecules of the target, this effect eventually must become important as the energy is decreased. I will introduce the modification version for the cross-section at lower energy in Subsection [IID](#).

B. Numerical integration of the rates

Except around narrow resonances, the S -factor is a smooth function of energy, which is suitable for extrapolating measured cross-sections down to astrophysical energies [5, 23, 28]. If the $S(E)$ is considered constant, the integrand in Eq. (2) is peaked at the "most effective energy" (also known as Gamow energy) [5, 23, 26, 29]

$$E_0 = \left(\frac{\mu}{2} \right)^{1/3} \left(\frac{\pi e^2 Z_1 Z_2 k_B T}{\hbar} \right)^{2/3} = 0.1220 (Z_1^2 Z_2^2 A)^{1/3} T_9^{2/3} \quad (5)$$

and might be estimated by a Gaussian function centered at E_0 , with full width at $1/e$ of the maximum provided by

$$\Delta E_0 = 4 \left(\frac{E_0 k_B T}{3} \right)^{1/2} = 0.2368 (Z_1^2 Z_2^2 A)^{1/6} T_9^{5/6}. \quad (6)$$

It is possible to calculate the integral in Eq. (2) analytically with these assumptions [5, 23, 26]. However, in this work, we did not stop at these approximations and performed the integral in Eq. (2) numerically, for the non-resonant contribution to the rate. For a given temperature, the integration is done to the energy domain $(E_0 - n' \Delta E_0, E_0 + n' \Delta E_0)$, with $n' = 2$ (as in Refs. [5, 23]) employing the 16-point Gaussian quadrature rule.

C. Electron screening by fusion plasma particles

Essentially, plasmas studied in fusion research are quasi-neutral, but there is a characteristic scale length for shielding the potential due to individual charges, that is known as the Debye screening length, and depends equally on the plasma's temperature and density. Since the mass ratio $m_D/m_e \gg 1$, electrons respond to the perturbations much faster than deuterons (ions), and the ions can be considered as background stationary particles to some degree, i.e., the effective density n_e of the free charge carriers (electrons) forms a Debye sphere λ_{De} around the deuterons, which leads to generating the screening potential. Therefore, the characteristic length of plasma for shielding, Debye screening length is determined by

$$\lambda_{De} = \left(\frac{k_B T_e}{4\pi n_e e^2} \right)^{1/2}. \quad (7)$$

Also, the electron screening, or, to be more accurate, the plasma-particle screening potential energy U_e can be written as

$$U_e = \frac{e^2}{\lambda_{De}}. \quad (8)$$

Similarly, the electron density (in cm^{-3}) regarding temperature and screening potential is

$$n_e = U_e^2 \frac{0.08617}{4\pi e^6} T_9 \times 10^{27} \simeq 2.3 \times 10^{24} U_e^2 T_9. \quad (9)$$

In Ref. [13] Schenkel et al. reported results for D-D fusion with palladium wires where D-D fusion reactions are studied in a pulsed plasma in the glow discharge regime using a benchtop apparatus. They found neutron yields as a function of cathode voltage over 100 times higher than yields expected for bare nuclei fusion at ion energies below 2 keV (center of mass frame). A possible explanation is a correction to the ion energy due to an electron screening potential. In comparison to neutron yield predictions with a series of values for the electron screening potential, they estimate $U_e = 1000 \pm 250$ eV in their experiments.

Accordingly, in this work, the calculations are performed for electron screening potentials of 100, 400, 750, 1000 eV and 1250 eV where the corresponding electron Debye length λ_{De} in Eq. (8) are equal to 1.4×10^{-9} , 3.6×10^{-10} , 1.9×10^{-10} , 1.4×10^{-10} and 1.1×10^{-10} cm, respectively.

D. Non-resonant data and extrapolation to astrophysical energies

For the extrapolation of the data points to zero energy, the laboratory cross-sections have to be corrected for electron screening [30] before employing them in the calculations of the rates. This effect becomes significant typically for $E/U_e \leq 100$. On the other hand, in stellar conditions, the nuclei are surrounded by a dense electron gas that reduces the Coulomb repulsion and makes penetration of the Coulomb barrier easier. The cross-sections are enhanced in comparison with the cross-sections between bare nuclei. This stellar screening effect can be described by applying, for example, the Debye-Huckel theory of dilute solutions of electrolytes [31]. The link between stellar and laboratory conditions therefore requires the bare-nucleus cross-sections.

The enhancement factor $f(E)$ due to electron screening is defined as [29]

$$f(E) = \frac{\sigma_{scr}(E)}{\sigma(E)} = \frac{\sigma(E + U_e)}{\sigma(E)}, \quad (10)$$

where $\sigma_{scr}(E)$ and $\sigma(E)$ are the cross-sections for the screened and the bare nuclei, respectively. The former is measured experimentally, and the latter can be obtained theoretically. When $U_e \ll E$, one can approximate the Eq. (10) by [5, 23]

$$f(E) \simeq \exp(\pi\eta U_e/E) \quad U_e \ll E. \quad (11)$$

The screened nuclear reaction cross-section can be expressed as [15, 32]

$$\sigma_{scr}(E) = \frac{1}{\sqrt{E(E + U_e)}} S(E) \exp\left(-2\pi\eta\sqrt{\frac{E}{E + U_e}}\right). \quad (12)$$

The early measurements of the screening energies for heavy metals was about 300 eV [6] which exceeded somewhat three times the theoretical predictions and also were significantly larger than the value $U_e = 20 \pm 5$ that measured for the gaseous targets [8, 9, 12]. Therefore, we also present our results for the screening energies of 100 and 400 eV, which correspond to the lower (theoretical) and upper (experimental) limit values same as Czerski did in [15].

In Ref. [5], the non-resonant data points (from either one or several publications) are represented in terms of S -factor data points, and then they performed the fit on the S -factor data by a polynomial as

$$S(E) \simeq \sum_{i=0}^N S_i E^i \quad (13)$$

Compilation	$p^3\text{H}$	$n^3\text{He}$
\mathcal{S}_0	56.0	55.0
NACRE	\mathcal{S}_1	0.204
	\mathcal{S}_2	-0.0251×10^{-3} -0.094×10^{-3}

TABLE I: The S function's fit coefficients, \mathcal{S}_0 (in keV.b), $\mathcal{S}_1 \equiv \alpha \mathcal{S}_0$ (in b) and \mathcal{S}_2 (in keV $^{-1}$ b) for the data set, NACRE [5]. The corresponding fitted function is given by the Eq. (13).

The degree of polynomial N can be chosen in such a way as to improve the quality of the fit, practically, the common values are $N = 2$ or 3 . The coefficients \mathcal{S}_i of this polynomial are taken straight from Ref. [5] for the $^2\text{H}(d, p)^3\text{H}$ and $^2\text{H}(d, n)^3\text{He}$ reactions, and they are indicated in Table I as the NACRE compilation. These coefficients were obtained from a χ^2 -fit, where the individual data points are weighted by the errors, as explained in Ref. [5].

The range of temperature over which the reaction rate is valid depends on how high an energy E_d the linear fit to S for those data is performed. If one considers the range of validity of the fit to end at the highest energy, i.e., $E_d = 120$ keV then, by inspecting the integrand of the reactivity integral, Eq. (3) would be applicable only in the range $kT = 0 - 6$ keV or equivalently, $0 - 1.4 T_9$ [28].

III. NUMERICAL RESULTS

Figure 1 presents the cross-sections of (a) $^2\text{H}(d, p)^3\text{H}$ and (b) $^2\text{H}(d, n)^3\text{He}$ reactions as given by Eq. (12) versus deuteron bombarding energy, E_d . The curves are evaluated for the screening energies of $U_e = 1250$ eV (solid brown line), $U_e = 1000$ eV (short dashed red line), $U_e = 750$ eV (dotted magenta line) and $U_e = 400$ eV (dash-dotted green line), $U_e = 100$ eV (dash-dot-dotted blue line). The first three values are predicted in the Ref. [13], whereas the fourth and fifth values are suggested in the Ref. [15] to the lower (theoretical) and upper (experimental) limit values, respectively. Also, for comparison, the results without considering the screening effects, i.e., $U_e = 0.0$ (dashed black line) are presented.

Our numerical results of the reaction rates with and without the screening effects as

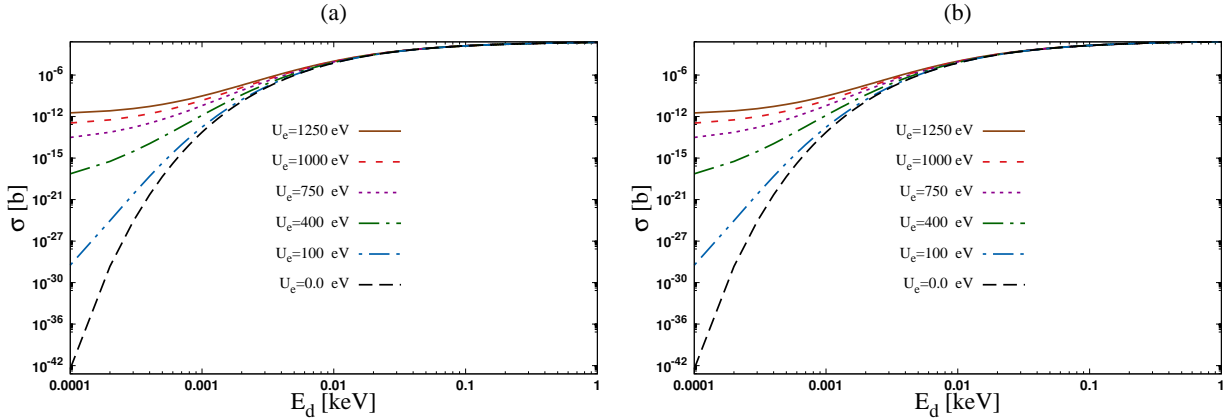


FIG. 1: The σ , cross-sections of (a) ${}^2\text{H}(d, p){}^3\text{H}$ and (b) ${}^2\text{H}(d, n){}^3\text{He}$ reactions as given by Eq. (12) for $U_e = 1250$ eV (solid brown line), $U_e = 1000$ eV (short dashed red line), $U_e = 750$ eV (dotted magenta line) from [13] and for $U_e = 400$ eV (dash-dotted green line), $U_e = 100$ eV (dash-dot-dotted blue line) from [15] and without considering the screening effects, i.e., $U_e = 0.0$ (dashed black line).

explained in Section II are given in a tabular way in Tables II and III as a function of T_9 . The temperature steps are the same as in [5, 23]. The reaction rates are expressed in $\text{cm}^3\text{mol}^{-1} \text{s}^{-1}$. The column *ratio* displays the ratios between with and without the screening effects rates. The column labeled *NACRE* indicates the ratios between this work's rate (without screening) and the rates proposed by [5]. The ${}^2\text{H}(d, p){}^3\text{H}$ and ${}^2\text{H}(d, n){}^3\text{He}$ reaction rates are calculated for $U_e = 100, 400$ eV, and the results are given in Tables II and III, respectively.

In the tables, we have not given the reaction rate results for values smaller than $N_A \langle \sigma v \rangle \leq 10^{-25} \text{ cm}^3\text{mol}^{-1} \text{s}^{-1}$. As mentioned in Ref. [5] the compilation is provided only with the reaction rates that are sufficiently large for the target lifetime to be shorter than the age of the Universe, 15×10^9 y, that leads to the lowest temperature T_9 is taken as 0.001.

By comparing the ${}^2\text{H}(d, p){}^3\text{H}$ reaction rates for $U_e = 100$ and $U_e = 400$ eV as given, in Table II, we see that at small T_9 there is a little enhancement in reaction rates for $U_e = 100$ eV, that is about 3 at $T_9 = 0.001$ while there is a significant increase for $U_e = 400$ eV, that is about 84 at $T_9 = 0.001$. It is also seen that with increasing temperature, $T_9 = 0.001$, this rate enhancement decreases until it becomes equal to the reaction rate without considering the screening effects. Therefore, as it was expected, the screening effects show itself at relatively

small energy and temperature. Also, the numerical results show the same behavior for ${}^2\text{H}(d, n){}^3\text{He}$ reaction rates by $U_e = 100$ and $U_e = 400$ eV which are given in Table III. In addition, to benchmark our numerical calculation, we compared our results by the rates proposed by [5]. According to the values presented in a column labeled *NACRE* in Tables II and III, there is an excellent agreement between ours and NACRE rates as given in [5].

In Table IV the electron densities n_e in term of temperature T_9 correspond to screening potentials $U_e = 100$ and 400 eV in Eq. (9), are presented. There, values of T_9 have been chosen at which the reaction rates according to the Tables II and III have a relatively significant value. In an ideal plasma, there are many particles per Debye sphere, i.e.

$$N_D \equiv n_e \frac{4\pi}{3} \lambda_D^3 \gg 1. \quad (14)$$

The classical plasma theory is built on the postulation that $N_D \gg 1$. This implies the dominance of the bulk effects over collisions between particles. Nevertheless, where $N_D \leq 1$ is the same as here, screening effects are decreased, and collisions will control the particle dynamics.

Dense metallic deuterium plasmas- In the figure 4 of the Ref. [17], a phase diagram of the matter is given that shows the parameter space for various Fermi systems in a log-log plot of temperature versus carrier number density. According to that diagram, the metallic deuterium plasma (by reflectance of ~ 0.7) is formed approximately at $T \sim 11$ eV and carrier number density (electrons and holes likewise) $n \sim 10^{24} \text{ cm}^{-3}$. Around this region the Coulomb coupling loosen up as Γ in Eq. (1) approaches 1. Moreover, the fluid becomes moderately coupled plasma. Thus, the Debye length for this plasma might be $\lambda_D \sim 2.5 \times 10^{-9} \text{ cm}$, where the following relation is used,

$$\lambda_D = 743 \left(\frac{T_e}{eV} \right)^{1/2} \left(\frac{n_e}{cm^{-3}} \right)^{-1/2} \text{ cm.} \quad (15)$$

Also, employing Eq. (8) for dense metallic deuterium plasmas, the corresponding screening potential energy could be $U_e \sim 60$ eV. The reaction rates for this screening potential are presented in Table V. At temperature $T_9 = 0.001$ (10^6 K) the reaction rate with screening increases about 1.9.

Moreover, the reaction rates are calculated with the values of the screening potentials $U_e = 750, 1000$ and 1250 eV, which are predicted by Schenkel et al. [13, 33] and, respectively, the numerical results are presented in Tables VI, VII and VIII for the ${}^2\text{H}(d, n){}^3\text{He}$ reaction

rates. In the experiments done by Schenkel et al. [13, 33], D-D fusion reactions are studied in a pulsed plasma in the glow discharge regime using a benchtop apparatus. They detected neutrons from D-D reactions with scintillator-based detectors. For palladium targets, they found neutron yields as a function of cathode voltage over 100 times higher than yields expected for bare nuclei fusion at ion energies below 2 keV (center of mass frame). As a conclusion, they present a possible explanation can be a correction to the ion energy due to an electron screening potential. In comparison to neutron yield predictions with a series of values for the electron screening potential, they estimate $U_e = 1000 \pm 250$ eV in their experiments. Also, the reaction rates for the ${}^2\text{H}(d, p){}^3\text{H}$ by these values of electron screening potential, i.e., $U_e = 750, 1000$ and 1250 eV are given in Tables IX, X and XI, respectively. These data can be useful for future measurements, because the branch ratio between the $\text{p} + \text{T}$ and $\text{n} + {}^3\text{He}$ channels is going to be determined with future implementation of a proton detector [13].

Finally, in order to show the dependence of the reaction rate on the screening potential, U_e , we have calculated the ratio of the reaction rate with the screening potential ($\langle \sigma_{scr} v \rangle$) to the reaction rate without the screening potential ($\langle \sigma v \rangle$), as function of $U_e / (k_B T) = 11.605 U_e / T_9$ and the results are depicted in Fig. 2. Then, by fitting the results with an analytical function, explicitly, it is found that the changes in the reaction rate are as:

$$\frac{\langle \sigma_{scr} v \rangle}{\langle \sigma v \rangle} = \exp(4.70 + 6.50 U_e / T_9). \quad (16)$$

The results of this analysis are almost identical for both reactions ${}^2\text{H}(d, p){}^3\text{H}$ and ${}^2\text{H}(d, n){}^3\text{He}$. Several analytical expressions for the rate of reaction have been given so far, the most recent one which is recommended by Tumino et al. [25] is,

$$N_A \langle \sigma v \rangle = \exp \left[a_1 + a_2 T_9^{-1} + a_3 T_9^{-1/3} + a_4 T_9^{1/3} + a_5 T_9 + a_6 T_9^{5/3} + a_7 \ln(T_9) \right], \quad (17)$$

where parameters a_i are given in Table 2 of [25].

IV. SUMMARY AND CONCLUSIONS

We calculated the Maxwellian-averaged thermonuclear reaction rates for ${}^2\text{H}(d, p){}^3\text{H}$ and ${}^2\text{H}(d, n){}^3\text{He}$ reactions by considering the screening effects. In the highly screened environment, when the hot fusion fuel interacts with lattice nuclei the electron screening may play

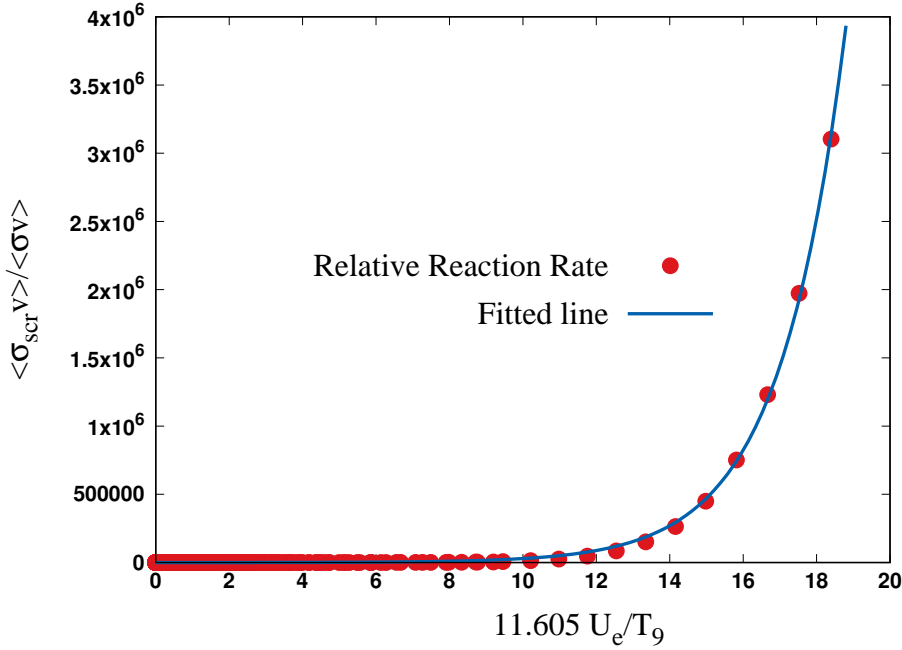


FIG. 2: The filled (red) circles show the relative reaction rate in Eq. (16) as function of $U_e / (k_B T) = 11.605 U_e/T_9$ for ${}^2\text{H}(d, p){}^3\text{H}$ and ${}^2\text{H}(d, n){}^3\text{He}$ reactions. This ratio is almost the same for both cases. The solid (blue) line shows the obtained fit function as given by the right-hand side of Eq. (16).

a significant role in tunneling through the Coulomb barrier. Under terrestrial conditions, it might be possible to simulate the D-D reactions in a metallic deuterium plasma in order to enhance the fusion rates at lower temperatures.

Firstly, we corrected the laboratory cross-sections for electron screening using the S-factor functions, which were obtained by fitting to low-energy data on ${}^2\text{H}(d, p){}^3\text{H}$ and ${}^2\text{H}(d, n){}^3\text{He}$ reactions. For this purpose, a fitted S-factor model based on the NACRE compilation is employed. Then, the integration of Eq. (3) is performed numerically to calculate the Maxwellian-averaged thermonuclear reaction rates. And, the corresponding rates of relevance in astrophysical plasmas at temperatures in the range from 10^6 K to 1.3×10^8 K are listed in a tabular way for a given screening energy. Where the values of screening energy motivated by the lower theoretical value 100 eV and upper experimental limit values 400, 750, 1000 eV and 1250 eV. In addition, the obtained rates were compared by the cases without screening and original NACRE results. Our numerical results showed a significant enhancement in reaction rate for both D-D reactions by screening energy ≥ 400

eV. This suggests that by using metallic deuterium plasma, it is possible to achieve higher reaction rates at lower temperatures.

Finally, the dependence of the reaction rate on the screening potential, U_e is investigated by calculating $\langle \sigma_{scr} v \rangle$ to $\langle \sigma v \rangle$, as function of $U_e / (k_B T) = 11.605 U_e / T_9$, and the results are fitted by an analytical function. Our numerical analysis suggests that this ratio can be well described by the term $\exp(4.70 + 6.50 U_e / T_9)$ for both $^2\text{H}(d, p)^3\text{H}$ and $^2\text{H}(d, n)^3\text{He}$ reactions. In conclusion, the screening potential can play a significant role in the reaction rate (depends on the temperature). The results of this work might help in the designing of future fusion experiments for the desired range of temperatures.

ACKNOWLEDGEMENT

The author gratefully acknowledges Dr. S. M. Khorashadizadeh for guidance and technical consultation regarding plasma physics.

REFERENCES

- [1] H.-S. Bosch and G. Hale, Improved formulas for fusion cross-sections and thermal reactivities, [Nucl. Fusion](#) **32**, 611 (1992).
- [2] S. Ichimaru, Nuclear fusion in dense plasmas, [Rev. Mod. Phys.](#) **65**, 255 (1993).
- [3] B. L. Whitten, N. F. Lane, and J. C. Weisheit, Plasma-screening effects on electron-impact excitation of hydrogenic ions in dense plasmas, [Phys. Rev. A](#) **29**, 945 (1984).
- [4] M. Aliotta and K. Langanke, Screening Effects in Stars and in the Laboratory, [Front. Phys.](#) **10**, [10.3389/fphy.2022.942726](https://doi.org/10.3389/fphy.2022.942726) (2022).
- [5] C. Angulo *et al.*, A compilation of charged-particle induced thermonuclear reaction rates, [Nuc. Phys. A](#) **656**, 3 (1999).
- [6] K. Czerski, A. Huke, A. Biller, P. Heide, M. Hoeft, and G. Ruprecht, Enhancement of the electron screening effect for $d + d$ fusion reactions in metallic environments, [Europhys. Lett.](#) **54**, 449 (2001).

- [7] F. Raiola *et al.*, Electron screening in d(d,p)t for deuterated metals and the periodic table, *Phys. Lett. B* **547**, 193 (2002).
- [8] F. Raiola, P. Migliardi, G. Gyürky, M. Aliotta, A. Formicola, R. Bonetti, C. Broggini, L. Campajola, P. Corvisiero, H. Costantini, *et al.*, Enhanced electron screening in d (d, p) t for deuterated Ta, *Eur. Phys. J. A-Hadrons and Nuclei* **13**, 377 (2002).
- [9] J. Kasagi, H. Yuki, T. Baba, T. Noda, J. Taguchi, M. Shimokawa, and W. Galster, Strongly Enhanced Li + D Reaction in Pd Observed in Deuteron Bombardment on $PdLi_x$ with Energies between 30 and 75 keV, *J. Phys. Soc. Jpn.* **73**, 608 (2004).
- [10] J. Cruz *et al.*, Electron screening in $^7Li(p,\alpha)\alpha$ and $^6Li(p,\alpha)^3He$ for different environments, *Phys. Lett. B* **624**, 181 (2005).
- [11] C. Bonomo *et al.*, Enhanced electron screening in d(d, p)t for deuterated metals: a possible classical explanation, *Nucl. Phys. A* **719**, C37 (2003).
- [12] U. Greife, F. Gorris, M. Junker, C. Rolfs, and D. Zahnow, Oppenheimer-Phillips effect and electron screening in d+ d fusion reactions, *Zeitschrift für Physik A Hadrons and Nuclei* **351**, 107 (1995).
- [13] T. Schenkel *et al.*, Investigation of light ion fusion reactions with plasma discharges, *J. Appl. Phys.* **126**, 203302 (2019).
- [14] A. Huke, K. Czerski, P. Heide, G. Ruprecht, N. Targosz, and W. Żebrowski, Enhancement of deuteron-fusion reactions in metals and experimental implications, *Phys. Rev. C* **78**, 015803 (2008).
- [15] K. Czerski, Deuteron-deuteron nuclear reactions at extremely low energies, *Phys. Rev. C* **106**, L011601 (2022).
- [16] M. D. Knudson, M. P. Desjarlais, A. Becker, R. W. Lemke, K. R. Cochrane, M. E. Savage, D. E. Bliss, T. R. Mattsson, and R. Redmer, Direct observation of an abrupt insulator-to-metal transition in dense liquid deuterium, *Sci.* **348**, 1455 (2015).
- [17] M. Zaghoo, T. R. Boehly, J. R. Rygg, P. M. Celliers, S. X. Hu, and G. W. Collins, Breakdown of Fermi Degeneracy in the Simplest Liquid Metal, *Phys. Rev. Lett.* **122**, 085001 (2019).
- [18] M. Zaghoo, R. J. Husband, and I. F. Silvera, Striking isotope effect on the metallization phase lines of liquid hydrogen and deuterium, *Phys. Rev. B* **98**, 104102 (2018).
- [19] K. Czerski *et al.*, Screening and resonance enhancements of the $^2H(d,p)^3H$ reaction yield in metallic environments, *Europhys. Lett.* **113**, 22001 (2016).

[20] A. Coc, P. Petitjean, J.-P. Uzan, E. Vangioni, P. Descouvemont, C. Iliadis, and R. Longland, New reaction rates for improved primordial D/H calculation and the cosmic evolution of deuterium, *Phys. Rev. D* **92**, 123526 (2015).

[21] R. H. Cyburt, Primordial nucleosynthesis for the new cosmology: Determining uncertainties and examining concordance, *Phys. Rev. D* **70**, 023505 (2004).

[22] P. D. Serpico, S. Esposito, F. Iocco, G. Mangano, G. Miele, and O. Pisanti, Nuclear reaction network for primordial nucleosynthesis: a detailed analysis of rates, uncertainties and light nuclei yields, *J. Cosmol. Astropart. Phys.* **2004** (12), 010.

[23] P. Descouvemont, A. Adahchour, C. Angulo, A. Coc, and E. Vangioni-Flam, Compilation and R-matrix analysis of Big Bang nuclear reaction rates, *At. Data Nucl. Data Tables* **88**, 203 (2004).

[24] D. S. Leonard, H. J. Karwowski, C. R. Brune, B. M. Fisher, and E. J. Ludwig, Precision measurements of $^2\text{H}(d, p)^3\text{H}$ and $^2\text{H}(d, n)^3\text{He}$ total cross sections at Big Bang nucleosynthesis energies, *Phys. Rev. C* **73**, 045801 (2006).

[25] A. Tumino, R. Spartà, C. Spitaleri, A. M. Mukhamedzhanov, S. Typel, R. G. Pizzone, E. Tognelli, S. Degl'Innocenti, V. Burjan, V. Kroha, Z. Hons, M. La Cognata, L. Lamia, J. Mrazek, S. Piskor, P. G. Prada Moroni, G. G. Rapisarda, S. Romano, and M. L. Sergi, New determination of the $^2\text{H}(d, p)^3\text{H}$ and $^2\text{H}(d, n)^3\text{He}$ reaction rates at astrophysical energies, *The Astrophysical Journal* **785**, 96 (2014).

[26] W. A. Fowler, G. R. Caughlan, and B. A. Zimmerman, Thermonuclear reaction rates, *Annu. Rev. Astron. Astrophys.* **5**, 525 (1967).

[27] E. M. Burbidge, G. R. Burbidge, W. A. Fowler, and F. Hoyle, Synthesis of the Elements in Stars, *Rev. Mod. Phys.* **29**, 547 (1957).

[28] R. E. Brown and N. Jarmie, Differential cross sections at low energies for $^2\text{H}(d, p)^3\text{H}$ and $^2\text{H}(d, n)^3\text{He}$, *Phys. Rev. C* **41**, 1391 (1990).

[29] V. Pines, M. Pines, A. Chait, B. M. Steinmetz, L. P. Forsley, R. C. Hendricks, G. C. Fralick, T. L. Benyo, B. Baramsai, P. B. Ugorowski, M. D. Becks, R. E. Martin, N. Penney, and C. E. Sandifer, Nuclear fusion reactions in deuterated metals, *Phys. Rev. C* **101**, 044609 (2020).

[30] H. Assenbaum, K. Langanke, and C. Rolfs, Effects of electron screening on low-energy fusion cross sections, *Zeitschrift für Physik A Atomic Nuclei* **327**, 461 (1987).

[31] P. Debye and E. Hückel, The Theory of Electrolytes I. Lowering of Freezing Point and Related Phenomena, *Physikalische Zeitschrift* **24**, 185 (1923).

[32] K. Czerski, A. Huke, P. Heide, and G. Ruprecht, The $^2H(d, p)^3H$ reaction in metallic media at very low energies, *Europhys. Lett.* **68**, 363 (2004).

[33] C. P. Berlinguette *et al.*, Revisiting the cold case of cold fusion, *Nature* **570**, 45 (2019).

TABLE II: The $^2H(d, p)^3H$ reaction rates ($\text{cm}^3\text{mol}^{-1} \text{s}^{-1}$). The corresponding electron Debye length λ_{De} (Eq. (8)) are equal to 1.4×10^{-9} and 3.6×10^{-10} cm for screening potentials $U_e = 100$ and 400 eV, respectively.

T_9	$U_e = 100 \text{ eV}$				$U_e = 400 \text{ eV}$			
	with screening	without screening	ratio	NACRE	with screening	without screening	ratio	NACRE
0.001	4.32E-08	1.42E-08	3.0	1.0	1.20E-06	1.42E-08	84.7	1.0
0.002	1.02E-04	5.88E-05	1.7	1.0	5.32E-04	5.88E-05	9.0	1.0
0.003	4.65E-03	3.23E-03	1.4	1.0	1.39E-02	3.23E-03	4.3	1.0
0.004	5.22E-02	3.99E-02	1.3	1.0	1.18E-01	3.99E-02	3.0	1.0
0.005	2.92E-01	2.36E-01	1.2	1.0	5.60E-01	2.36E-01	2.4	1.0
0.006	1.09E+00	9.09E-01	1.2	1.0	1.87E+00	9.09E-01	2.1	1.0
0.007	3.10E+00	2.66E+00	1.2	1.0	4.91E+00	2.66E+00	1.8	1.0
0.008	7.34E+00	6.43E+00	1.1	1.0	1.10E+01	6.43E+00	1.7	1.0
0.009	1.52E+01	1.35E+01	1.1	1.0	2.17E+01	1.35E+01	1.6	1.0
0.010	2.85E+01	2.56E+01	1.1	1.0	3.92E+01	2.56E+01	1.5	1.0
0.011	4.92E+01	4.47E+01	1.1	1.0	6.57E+01	4.47E+01	1.5	1.0
0.012	7.97E+01	7.31E+01	1.1	1.0	1.04E+02	7.31E+01	1.4	1.0
0.013	1.23E+02	1.13E+02	1.1	1.0	1.57E+02	1.13E+02	1.4	1.0
0.014	1.81E+02	1.68E+02	1.1	1.0	2.27E+02	1.68E+02	1.4	1.0
0.015	2.57E+02	2.40E+02	1.1	1.0	3.18E+02	2.40E+02	1.3	1.0
0.016	3.55E+02	3.33E+02	1.1	1.0	4.33E+02	3.33E+02	1.3	1.0
0.018	6.27E+02	5.93E+02	1.1	1.0	7.47E+02	5.93E+02	1.3	1.0
0.020	1.02E+03	9.71E+02	1.1	1.0	1.19E+03	9.71E+02	1.2	1.0
0.025	2.70E+03	2.60E+03	1.0	1.0	3.06E+03	2.60E+03	1.2	1.0
0.030	5.65E+03	5.47E+03	1.0	1.0	6.26E+03	5.47E+03	1.1	1.0
0.040	1.64E+04	1.60E+04	1.0	1.0	1.77E+04	1.60E+04	1.1	1.0
0.050	3.48E+04	3.42E+04	1.0	1.0	3.69E+04	3.42E+04	1.1	1.0
0.060	6.14E+04	6.05E+04	1.0	1.0	6.45E+04	6.05E+04	1.1	1.0
0.070	9.64E+04	9.51E+04	1.0	1.0	1.00E+05	9.51E+04	1.1	1.0
0.080	1.39E+05	1.38E+05	1.0	1.0	1.45E+05	1.38E+05	1.0	1.0
0.090	1.90E+05	1.88E+05	1.0	1.0	1.96E+05	1.88E+05	1.0	1.0
0.100	2.48E+05	2.46E+05	1.0	1.0	2.55E+05	2.46E+05	1.0	1.0
0.110	3.13E+05	3.10E+05	1.0	1.0	3.21E+05	3.10E+05	1.0	1.0
0.120	3.83E+05	3.81E+05	1.0	1.0	3.93E+05	3.81E+05	1.0	1.0
0.130	4.60E+05	4.57E+05	1.0	1.0	4.70E+05	4.57E+05	1.0	1.0

TABLE III: The $^2\text{H}(d, n)^3\text{He}$ reaction rates ($\text{cm}^3\text{mol}^{-1} \text{s}^{-1}$).

T_9	$U_e = 100 \text{ eV}$				$U_e = 400 \text{ eV}$					
	with screening		without	ratio	NACRE	with screening		without	ratio	NACRE
		screening					screening			
0.001	4.26E-08	1.40E-08	3.0	1.0		1.18E-06	1.40E-08	84.6	1.0	
0.002	1.01E-04	5.80E-05	1.7	1.0		5.24E-04	5.80E-05	9.0	1.0	
0.003	4.59E-03	3.19E-03	1.4	1.0		1.37E-02	3.19E-03	4.3	1.0	
0.004	5.16E-02	3.94E-02	1.3	1.0		1.17E-01	3.94E-02	3.0	1.0	
0.005	2.89E-01	2.33E-01	1.2	1.0		5.54E-01	2.33E-01	2.4	1.0	
0.006	1.08E+00	9.01E-01	1.2	1.0		1.85E+00	9.01E-01	2.1	1.0	
0.007	3.07E+00	2.64E+00	1.2	1.0		4.87E+00	2.64E+00	1.8	1.0	
0.008	7.28E+00	6.38E+00	1.1	1.0		1.09E+01	6.38E+00	1.7	1.0	
0.009	1.51E+01	1.34E+01	1.1	1.0		2.16E+01	1.34E+01	1.6	1.0	
0.010	2.83E+01	2.55E+01	1.1	1.0		3.89E+01	2.55E+01	1.5	1.0	
0.011	4.89E+01	4.45E+01	1.1	1.0		6.53E+01	4.45E+01	1.5	1.0	
0.012	7.94E+01	7.28E+01	1.1	1.0		1.03E+02	7.28E+01	1.4	1.0	
0.013	1.22E+02	1.13E+02	1.1	1.0		1.56E+02	1.13E+02	1.4	1.0	
0.014	1.80E+02	1.68E+02	1.1	1.0		2.26E+02	1.68E+02	1.3	1.0	
0.015	2.57E+02	2.40E+02	1.1	1.0		3.17E+02	2.40E+02	1.3	1.0	
0.016	3.55E+02	3.33E+02	1.1	1.0		4.32E+02	3.33E+02	1.3	1.0	
0.018	6.27E+02	5.93E+02	1.1	1.0		7.46E+02	5.93E+02	1.3	1.0	
0.020	1.02E+03	9.72E+02	1.1	1.0		1.20E+03	9.72E+02	1.2	1.0	
0.025	2.72E+03	2.61E+03	1.0	1.0		3.07E+03	2.61E+03	1.2	1.0	
0.030	5.69E+03	5.51E+03	1.0	1.0		6.31E+03	5.51E+03	1.1	1.0	
0.040	1.66E+04	1.62E+04	1.0	1.0		1.79E+04	1.62E+04	1.1	1.0	
0.050	3.54E+04	3.48E+04	1.0	1.0		3.76E+04	3.48E+04	1.1	1.0	
0.060	6.28E+04	6.18E+04	1.0	1.0		6.59E+04	6.18E+04	1.1	1.0	
0.070	9.89E+04	9.77E+04	1.0	1.0		1.03E+05	9.77E+04	1.1	1.0	
0.080	1.44E+05	1.42E+05	1.0	1.0		1.49E+05	1.42E+05	1.0	1.0	
0.090	1.97E+05	1.95E+05	1.0	1.0		2.03E+05	1.95E+05	1.0	1.0	
0.100	2.58E+05	2.55E+05	1.0	1.0		2.65E+05	2.55E+05	1.0	1.0	
0.110	3.26E+05	3.23E+05	1.0	1.0		3.34E+05	3.23E+05	1.0	1.0	
0.120	4.01E+05	3.98E+05	1.0	1.0		4.10E+05	3.98E+05	1.0	1.0	
0.130	4.82E+05	4.79E+05	1.0	1.0		4.92E+05	4.79E+05	1.0	1.0	

TABLE IV: The electron density n_e (in cm^{-3}) versus temperature T_9 for two fixed value of screening potential $U_e = 100$ and 400 eV as given by Eq. (9).

T_9	0.001	0.002	0.003	0.004	0.005	0.006	0.007	0.008	0.009	0.010	
n_e	$U_e = 100$	2.30E+25	4.59E+25	6.89E+25	9.19E+25	1.15E+26	1.38E+26	1.61E+26	1.84E+26	2.07E+26	2.30E+26
	$U_e = 400$	3.67E+26	7.35E+26	1.10E+27	1.47E+27	1.84E+27	2.20E+27	2.57E+27	2.94E+27	3.31E+27	3.67E+27

TABLE V: The ${}^2\text{H}(d, p){}^3\text{H}$ reaction rates ($\text{cm}^3\text{mol}^{-1} \text{s}^{-1}$) for $U_e = 60 \text{ eV}$; and
 $\lambda_{De} = 2.4 \times 10^{-9} \text{ cm}$.

T_9	with	without	ratio	T_9	with	without	ratio
	screening	screening			screening	screening	
10 ⁻⁵	3.72E-49	1.35E-74	2.76E+25	0.009	1.45E+01	1.35E+01	1.1
10 ⁻⁴	2.68E-26	2.91E-29	9.20E+02	0.010	2.73E+01	2.56E+01	1.1
0.001	2.77E-08	1.42E-08	1.9	0.011	4.73E+01	4.47E+01	1.1
0.002	8.17E-05	5.88E-05	1.4	0.012	7.69E+01	7.31E+01	1.1
0.003	4.02E-03	3.23E-03	1.2	0.013	1.19E+02	1.13E+02	1.0
0.004	4.68E-02	3.99E-02	1.2	0.014	1.76E+02	1.68E+02	1.0
0.005	2.68E-01	2.36E-01	1.1	0.015	2.50E+02	2.40E+02	1.0
0.006	1.01E+00	9.09E-01	1.1	0.016	3.46E+02	3.33E+02	1.0
0.007	2.91E+00	2.66E+00	1.1	0.018	6.13E+02	5.93E+02	1.0
0.008	6.96E+00	6.43E+00	1.1	0.020	1.00E+03	9.71E+02	1.0

TABLE VI: The ${}^2\text{H}(d, n){}^3\text{He}$ reaction rates ($\text{cm}^3\text{mol}^{-1} \text{s}^{-1}$) for $U_e = 750 \text{ eV}$; and
 $\lambda_{De} = 1.9 \times 10^{-10} \text{ cm}$.

T_9	with screening	without	ratio	n_e	T_9	with screening	without	ratio	n_e
	screening	screening				screening	screening		
0.001	5.09E-05	1.40E-08	3639.8	1.29E+15	0.140	5.94E+05	5.66E+05	1.0	1.81E+17
0.002	3.50E-03	5.80E-05	60.4	2.58E+15	0.150	6.88E+05	6.59E+05	1.0	1.94E+17
0.003	4.85E-02	3.19E-03	15.2	3.88E+15	0.160	7.88E+05	7.56E+05	1.0	2.07E+17
0.004	3.00E-01	3.94E-02	7.6	5.17E+15	0.180	1.00E+06	9.65E+05	1.0	2.33E+17
0.005	1.18E+00	2.33E-01	5.0	6.46E+15	0.200	1.23E+06	1.19E+06	1.0	2.58E+17
0.006	3.45E+00	9.01E-01	3.8	7.75E+15	0.250	1.85E+06	1.81E+06	1.0	3.23E+17
0.007	8.31E+00	2.64E+00	3.1	9.04E+15	0.300	2.53E+06	2.48E+06	1.0	3.88E+17
0.008	1.74E+01	6.38E+00	2.7	1.03E+16	0.350	3.25E+06	3.19E+06	1.0	4.52E+17
0.009	3.26E+01	1.34E+01	2.4	1.16E+16	0.400	3.99E+06	3.93E+06	1.0	5.17E+17
0.010	5.64E+01	2.55E+01	2.2	1.29E+16	0.450	4.75E+06	4.69E+06	1.0	5.81E+17
0.011	9.15E+01	4.45E+01	2.1	1.42E+16	0.500	5.52E+06	5.46E+06	1.0	6.46E+17
0.012	1.41E+02	7.28E+01	1.9	1.55E+16	0.600	7.07E+06	7.01E+06	1.0	7.75E+17
0.013	2.07E+02	1.13E+02	1.8	1.68E+16	0.700	8.63E+06	8.57E+06	1.0	9.04E+17
0.014	2.94E+02	1.68E+02	1.8	1.81E+16	0.800	1.02E+07	1.01E+07	1.0	1.03E+18
0.015	4.05E+02	2.40E+02	1.7	1.94E+16	0.900	1.17E+07	1.16E+07	1.0	1.16E+18
0.016	5.43E+02	3.33E+02	1.6	2.07E+16	1.000	1.32E+07	1.31E+07	1.0	1.29E+18
0.018	9.13E+02	5.93E+02	1.5	2.33E+16	1.250	1.68E+07	1.68E+07	1.0	1.61E+18
0.020	1.43E+03	9.72E+02	1.5	2.58E+16	1.500	2.02E+07	2.02E+07	1.0	1.94E+18
0.025	3.55E+03	2.61E+03	1.4	3.23E+16	1.750	2.35E+07	2.34E+07	1.0	2.26E+18
0.030	7.10E+03	5.51E+03	1.3	3.88E+16	2.000	2.65E+07	2.65E+07	1.0	2.58E+18
0.040	1.96E+04	1.62E+04	1.2	5.17E+16	2.500	3.21E+07	3.20E+07	1.0	3.23E+18
0.050	4.03E+04	3.48E+04	1.2	6.46E+16	3.000	3.70E+07	3.70E+07	1.0	3.88E+18
0.060	6.98E+04	6.18E+04	1.1	7.75E+16	3.500	4.13E+07	4.13E+07	1.0	4.52E+18
0.070	1.08E+05	9.77E+04	1.1	9.04E+16	4.000	4.51E+07	4.51E+07	1.0	5.17E+18
0.080	1.55E+05	1.42E+05	1.1	1.03E+17	5.000	5.14E+07	5.14E+07	1.0	6.46E+18
0.090	2.11E+05	1.95E+05	1.1	1.16E+17	6.000	5.60E+07	5.60E+07	1.0	7.75E+18
0.100	2.74E+05	2.55E+05	1.1	1.29E+17	7.000	5.92E+07	5.92E+07	1.0	9.04E+18
0.110	3.44E+05	3.23E+05	1.1	1.42E+17	8.000	6.11E+07	6.11E+07	1.0	1.03E+19
0.120	4.21E+05	3.98E+05	1.1	1.55E+17	9.000	6.20E+07	6.20E+07	1.0	1.16E+19
0.130	5.05E+05	4.79E+05	1.1	1.68E+17	10.000	6.18E+07	6.18E+07	1.0	1.29E+19

TABLE VII: The ${}^2\text{H}(d, n){}^3\text{He}$ reaction rates ($\text{cm}^3\text{mol}^{-1} \text{s}^{-1}$) for $U_e = 1000 \text{ eV}$; and $\lambda_{De} = 1.4 \times 10^{-10} \text{ cm}$.

T_9	with screening	without screening	ratio	n_e	T_9	with screening	without screening	ratio	n_e
0.001	5.81E-04	1.40E-08	41530.7	2.30E+15	0.140	6.03E+05	5.66E+05	1.1	3.22E+17
0.002	1.32E-02	5.80E-05	227.6	4.59E+15	0.150	6.99E+05	6.59E+05	1.1	3.44E+17
0.003	1.18E-01	3.19E-03	37.0	6.89E+15	0.160	7.99E+05	7.56E+05	1.1	3.67E+17
0.004	5.86E-01	3.94E-02	14.9	9.19E+15	0.180	1.01E+06	9.65E+05	1.0	4.13E+17
0.005	2.01E+00	2.33E-01	8.6	1.15E+16	0.200	1.24E+06	1.19E+06	1.0	4.59E+17
0.006	5.38E+00	9.01E-01	6.0	1.38E+16	0.250	1.87E+06	1.81E+06	1.0	5.74E+17
0.007	1.21E+01	2.64E+00	4.6	1.61E+16	0.300	2.55E+06	2.48E+06	1.0	6.89E+17
0.008	2.42E+01	6.38E+00	3.8	1.84E+16	0.350	3.26E+06	3.19E+06	1.0	8.04E+17
0.009	4.37E+01	1.34E+01	3.3	2.07E+16	0.400	4.01E+06	3.93E+06	1.0	9.19E+17
0.010	7.34E+01	2.55E+01	2.9	2.30E+16	0.450	4.77E+06	4.69E+06	1.0	1.03E+18
0.011	1.16E+02	4.45E+01	2.6	2.53E+16	0.500	5.54E+06	5.46E+06	1.0	1.15E+18
0.012	1.75E+02	7.28E+01	2.4	2.76E+16	0.600	7.09E+06	7.01E+06	1.0	1.38E+18
0.013	2.53E+02	1.13E+02	2.2	2.99E+16	0.700	8.65E+06	8.57E+06	1.0	1.61E+18
0.014	3.54E+02	1.68E+02	2.1	3.22E+16	0.800	1.02E+07	1.01E+07	1.0	1.84E+18
0.015	4.81E+02	2.40E+02	2.0	3.44E+16	0.900	1.17E+07	1.16E+07	1.0	2.07E+18
0.016	6.38E+02	3.33E+02	1.9	3.67E+16	1.000	1.32E+07	1.31E+07	1.0	2.30E+18
0.018	1.05E+03	5.93E+02	1.8	4.13E+16	1.250	1.68E+07	1.68E+07	1.0	2.87E+18
0.020	1.63E+03	9.72E+02	1.7	4.59E+16	1.500	2.02E+07	2.02E+07	1.0	3.44E+18
0.025	3.93E+03	2.61E+03	1.5	5.74E+16	1.750	2.35E+07	2.34E+07	1.0	4.02E+18
0.030	7.73E+03	5.51E+03	1.4	6.89E+16	2.000	2.65E+07	2.65E+07	1.0	4.59E+18
0.040	2.08E+04	1.62E+04	1.3	9.19E+16	2.500	3.21E+07	3.20E+07	1.0	5.74E+18
0.050	4.23E+04	3.48E+04	1.2	1.15E+17	3.000	3.70E+07	3.70E+07	1.0	6.89E+18
0.060	7.27E+04	6.18E+04	1.2	1.38E+17	3.500	4.13E+07	4.13E+07	1.0	8.04E+18
0.070	1.12E+05	9.77E+04	1.1	1.61E+17	4.000	4.52E+07	4.51E+07	1.0	9.19E+18
0.080	1.60E+05	1.42E+05	1.1	1.84E+17	5.000	5.14E+07	5.14E+07	1.0	1.15E+19
0.090	2.16E+05	1.95E+05	1.1	2.07E+17	6.000	5.60E+07	5.60E+07	1.0	1.38E+19
0.100	2.80E+05	2.55E+05	1.1	2.30E+17	7.000	5.92E+07	5.92E+07	1.0	1.61E+19
0.110	3.51E+05	3.23E+05	1.1	2.53E+17	8.000	6.12E+07	6.11E+07	1.0	1.84E+19
0.120	4.29E+05	3.98E+05	1.1	2.76E+17	9.000	6.20E+07	6.20E+07	1.0	2.07E+19
0.130	5.13E+05	4.79E+05	1.1	2.99E+17	10.000	6.18E+07	6.18E+07	1.0	2.30E+19

TABLE VIII: The ${}^2\text{H}(d, n){}^3\text{He}$ reaction rates ($\text{cm}^3\text{mol}^{-1} \text{s}^{-1}$) for $U_e = 1250 \text{ eV}$; and $\lambda_{De} = 1.1 \times 10^{-10} \text{ cm}$.

T_9	with screening	without screening	ratio	n_e	T_9	with screening	without screening	ratio	n_e
0.001	4.63E-03	1.40E-08	3.3E+05	3.59E+15	0.140	6.13E+05	5.66E+05	1.1	5.02E+17
0.002	4.72E-02	5.80E-05	813.7	7.18E+15	0.150	7.09E+05	6.59E+05	1.1	5.38E+17
0.003	2.83E-01	3.19E-03	88.7	1.08E+16	0.160	8.10E+05	7.56E+05	1.1	5.74E+17
0.004	1.13E+00	3.94E-02	28.7	1.44E+16	0.180	1.02E+06	9.65E+05	1.1	6.46E+17
0.005	3.40E+00	2.33E-01	14.6	1.79E+16	0.200	1.25E+06	1.19E+06	1.1	7.18E+17
0.006	8.34E+00	9.01E-01	9.3	2.15E+16	0.250	1.88E+06	1.81E+06	1.0	8.97E+17
0.007	1.77E+01	2.64E+00	6.7	2.51E+16	0.300	2.56E+06	2.48E+06	1.0	1.08E+18
0.008	3.36E+01	6.38E+00	5.3	2.87E+16	0.350	3.28E+06	3.19E+06	1.0	1.26E+18
0.009	5.85E+01	1.34E+01	4.4	3.23E+16	0.400	4.03E+06	3.93E+06	1.0	1.44E+18
0.010	9.54E+01	2.55E+01	3.7	3.59E+16	0.450	4.79E+06	4.69E+06	1.0	1.61E+18
0.011	1.47E+02	4.45E+01	3.3	3.95E+16	0.500	5.56E+06	5.46E+06	1.0	1.79E+18
0.012	2.17E+02	7.28E+01	3.0	4.31E+16	0.600	7.11E+06	7.01E+06	1.0	2.15E+18
0.013	3.09E+02	1.13E+02	2.7	4.67E+16	0.700	8.67E+06	8.57E+06	1.0	2.51E+18
0.014	4.26E+02	1.68E+02	2.5	5.02E+16	0.800	1.02E+07	1.01E+07	1.0	2.87E+18
0.015	5.72E+02	2.40E+02	2.4	5.38E+16	0.900	1.17E+07	1.16E+07	1.0	3.23E+18
0.016	7.50E+02	3.33E+02	2.3	5.74E+16	1.000	1.32E+07	1.31E+07	1.0	3.59E+18
0.018	1.22E+03	5.93E+02	2.1	6.46E+16	1.250	1.68E+07	1.68E+07	1.0	4.49E+18
0.020	1.85E+03	9.72E+02	1.9	7.18E+16	1.500	2.03E+07	2.02E+07	1.0	5.38E+18
0.025	4.35E+03	2.61E+03	1.7	8.97E+16	1.750	2.35E+07	2.34E+07	1.0	6.28E+18
0.030	8.41E+03	5.51E+03	1.5	1.08E+17	2.000	2.65E+07	2.65E+07	1.0	7.18E+18
0.040	2.22E+04	1.62E+04	1.4	1.44E+17	2.500	3.21E+07	3.20E+07	1.0	8.97E+18
0.050	4.44E+04	3.48E+04	1.3	1.79E+17	3.000	3.70E+07	3.70E+07	1.0	1.08E+19
0.060	7.57E+04	6.18E+04	1.2	2.15E+17	3.500	4.13E+07	4.13E+07	1.0	1.26E+19
0.070	1.16E+05	9.77E+04	1.2	2.51E+17	4.000	4.52E+07	4.51E+07	1.0	1.44E+19
0.080	1.65E+05	1.42E+05	1.2	2.87E+17	5.000	5.14E+07	5.14E+07	1.0	1.79E+19
0.090	2.22E+05	1.95E+05	1.1	3.23E+17	6.000	5.60E+07	5.60E+07	1.0	2.15E+19
0.100	2.87E+05	2.55E+05	1.1	3.59E+17	7.000	5.92E+07	5.92E+07	1.0	2.51E+19
0.110	3.59E+05	3.23E+05	1.1	3.95E+17	8.000	6.12E+07	6.11E+07	1.0	2.87E+19
0.120	4.38E+05	3.98E+05	1.1	4.31E+17	9.000	6.20E+07	6.20E+07	1.0	3.23E+19
0.130	5.23E+05	4.79E+05	1.1	4.67E+17	10.000	6.18E+07	6.18E+07	1.0	3.59E+19

TABLE IX: The ${}^2\text{H}(d, p){}^3\text{H}$ reaction rates ($\text{cm}^3\text{mol}^{-1} \text{s}^{-1}$) for $U_e = 750$ eV.

T_9	with screening	without screening	ratio	n_e	T_9	with screening	without screening	ratio	n_e
0.001	5.18E-05	1.42E-08	3644.7	1.29E+15	0.140	5.65E+05	5.38E+05	1.0	1.81E+17
0.002	3.56E-03	5.88E-05	60.5	2.58E+15	0.150	6.53E+05	6.25E+05	1.0	1.94E+17
0.003	4.92E-02	3.23E-03	15.2	3.88E+15	0.160	7.46E+05	7.15E+05	1.0	2.07E+17
0.004	3.04E-01	3.99E-02	7.6	5.17E+15	0.180	9.41E+05	9.08E+05	1.0	2.33E+17
0.005	1.19E+00	2.36E-01	5.1	6.46E+15	0.200	1.15E+06	1.11E+06	1.0	2.58E+17
0.006	3.49E+00	9.09E-01	3.8	7.75E+15	0.250	1.71E+06	1.67E+06	1.0	3.23E+17
0.007	8.39E+00	2.66E+00	3.2	9.04E+15	0.300	2.32E+06	2.27E+06	1.0	3.88E+17
0.008	1.75E+01	6.43E+00	2.7	1.03E+16	0.350	2.95E+06	2.90E+06	1.0	4.52E+17
0.009	3.29E+01	1.35E+01	2.4	1.16E+16	0.400	3.60E+06	3.55E+06	1.0	5.17E+17
0.010	5.68E+01	2.56E+01	2.2	1.29E+16	0.450	4.26E+06	4.21E+06	1.0	5.81E+17
0.011	9.21E+01	4.47E+01	2.1	1.42E+16	0.500	4.92E+06	4.87E+06	1.0	6.46E+17
0.012	1.41E+02	7.31E+01	1.9	1.55E+16	0.600	6.24E+06	6.18E+06	1.0	7.75E+17
0.013	2.08E+02	1.13E+02	1.8	1.68E+16	0.700	7.54E+06	7.49E+06	1.0	9.04E+17
0.014	2.95E+02	1.68E+02	1.8	1.81E+16	0.800	8.82E+06	8.77E+06	1.0	1.03E+18
0.015	4.06E+02	2.40E+02	1.7	1.94E+16	0.900	1.01E+07	1.00E+07	1.0	1.16E+18
0.016	5.44E+02	3.33E+02	1.6	2.07E+16	1.000	1.13E+07	1.13E+07	1.0	1.29E+18
0.018	9.15E+02	5.93E+02	1.5	2.33E+16	1.250	1.43E+07	1.42E+07	1.0	1.61E+18
0.020	1.43E+03	9.71E+02	1.5	2.58E+16	1.500	1.71E+07	1.70E+07	1.0	1.94E+18
0.025	3.54E+03	2.60E+03	1.4	3.23E+16	1.750	1.97E+07	1.97E+07	1.0	2.26E+18
0.030	7.06E+03	5.47E+03	1.3	3.88E+16	2.000	2.22E+07	2.22E+07	1.0	2.58E+18
0.040	1.93E+04	1.60E+04	1.2	5.17E+16	2.500	2.69E+07	2.68E+07	1.0	3.23E+18
0.050	3.96E+04	3.42E+04	1.2	6.46E+16	3.000	3.11E+07	3.11E+07	1.0	3.88E+18
0.060	6.83E+04	6.05E+04	1.1	7.75E+16	3.500	3.51E+07	3.50E+07	1.0	4.52E+18
0.070	1.06E+05	9.51E+04	1.1	9.04E+16	4.000	3.87E+07	3.87E+07	1.0	5.17E+18
0.080	1.51E+05	1.38E+05	1.1	1.03E+17	5.000	4.52E+07	4.52E+07	1.0	6.46E+18
0.090	2.04E+05	1.88E+05	1.1	1.16E+17	6.000	5.10E+07	5.10E+07	1.0	7.75E+18
0.100	2.64E+05	2.46E+05	1.1	1.29E+17	7.000	5.60E+07	5.60E+07	1.0	9.04E+18
0.110	3.31E+05	3.10E+05	1.1	1.42E+17	8.000	6.04E+07	6.04E+07	1.0	1.03E+19
0.120	4.03E+05	3.81E+05	1.1	1.55E+17	9.000	6.44E+07	6.44E+07	1.0	1.16E+19
0.130	4.82E+05	4.57E+05	1.1	1.68E+17	10.000	6.79E+07	6.79E+07	1.0	1.29E+19

TABLE X: The ${}^2\text{H}(d, p){}^3\text{H}$ reaction rates ($\text{cm}^3\text{mol}^{-1} \text{s}^{-1}$) for $U_e = 1000$ eV.

T_9	with screening	without screening	ratio	n_e	T_9	with screening	without screening	ratio	n_e
0.001	5.91E-04	1.42E-08	41598.9	2.30E+15	0.140	5.75E+05	5.38E+05	1.1	3.22E+17
0.002	1.34E-02	5.88E-05	228.0	4.59E+15	0.150	6.63E+05	6.25E+05	1.1	3.44E+17
0.003	1.20E-01	3.23E-03	37.1	6.89E+15	0.160	7.56E+05	7.15E+05	1.1	3.67E+17
0.004	5.94E-01	3.99E-02	14.9	9.19E+15	0.180	9.53E+05	9.08E+05	1.1	4.13E+17
0.005	2.03E+00	2.36E-01	8.6	1.15E+16	0.200	1.16E+06	1.11E+06	1.0	4.59E+17
0.006	5.44E+00	9.09E-01	6.0	1.38E+16	0.250	1.73E+06	1.67E+06	1.0	5.74E+17
0.007	1.23E+01	2.66E+00	4.6	1.61E+16	0.300	2.34E+06	2.27E+06	1.0	6.89E+17
0.008	2.44E+01	6.43E+00	3.8	1.84E+16	0.350	2.97E+06	2.90E+06	1.0	8.04E+17
0.009	4.41E+01	1.35E+01	3.3	2.07E+16	0.400	3.62E+06	3.55E+06	1.0	9.19E+17
0.010	7.40E+01	2.56E+01	2.9	2.30E+16	0.450	4.28E+06	4.21E+06	1.0	1.03E+18
0.011	1.17E+02	4.47E+01	2.6	2.53E+16	0.500	4.94E+06	4.87E+06	1.0	1.15E+18
0.012	1.76E+02	7.31E+01	2.4	2.76E+16	0.600	6.26E+06	6.18E+06	1.0	1.38E+18
0.013	2.55E+02	1.13E+02	2.2	2.99E+16	0.700	7.56E+06	7.49E+06	1.0	1.61E+18
0.014	3.56E+02	1.68E+02	2.1	3.22E+16	0.800	8.84E+06	8.77E+06	1.0	1.84E+18
0.015	4.83E+02	2.40E+02	2.0	3.44E+16	0.900	1.01E+07	1.00E+07	1.0	2.07E+18
0.016	6.40E+02	3.33E+02	1.9	3.67E+16	1.000	1.13E+07	1.13E+07	1.0	2.30E+18
0.018	1.06E+03	5.93E+02	1.8	4.13E+16	1.250	1.43E+07	1.42E+07	1.0	2.87E+18
0.020	1.63E+03	9.71E+02	1.7	4.59E+16	1.500	1.71E+07	1.70E+07	1.0	3.44E+18
0.025	3.92E+03	2.60E+03	1.5	5.74E+16	1.750	1.97E+07	1.97E+07	1.0	4.02E+18
0.030	7.68E+03	5.47E+03	1.4	6.89E+16	2.000	2.22E+07	2.22E+07	1.0	4.59E+18
0.040	2.06E+04	1.60E+04	1.3	9.19E+16	2.500	2.69E+07	2.68E+07	1.0	5.74E+18
0.050	4.16E+04	3.42E+04	1.2	1.15E+17	3.000	3.11E+07	3.11E+07	1.0	6.89E+18
0.060	7.12E+04	6.05E+04	1.2	1.38E+17	3.500	3.51E+07	3.50E+07	1.0	8.04E+18
0.070	1.09E+05	9.51E+04	1.1	1.61E+17	4.000	3.87E+07	3.87E+07	1.0	9.19E+18
0.080	1.55E+05	1.38E+05	1.1	1.84E+17	5.000	4.53E+07	4.52E+07	1.0	1.15E+19
0.090	2.09E+05	1.88E+05	1.1	2.07E+17	6.000	5.10E+07	5.10E+07	1.0	1.38E+19
0.100	2.70E+05	2.46E+05	1.1	2.30E+17	7.000	5.60E+07	5.60E+07	1.0	1.61E+19
0.110	3.38E+05	3.10E+05	1.1	2.53E+17	8.000	6.05E+07	6.04E+07	1.0	1.84E+19
0.120	4.11E+05	3.81E+05	1.1	2.76E+17	9.000	6.44E+07	6.44E+07	1.0	2.07E+19
0.130	4.90E+05	4.57E+05	1.1	2.99E+17	10.000	6.79E+07	6.79E+07	1.0	2.30E+19

TABLE XI: The ${}^2\text{H}(d, p){}^3\text{H}$ reaction rates ($\text{cm}^3\text{mol}^{-1} \text{s}^{-1}$) for $U_e = 1250$ eV.

T_9	with screening	without screening	ratio	n_e	T_9	with screening	without screening	ratio	n_e
0.001	4.71E-03	1.42E-08	3.3E+05	3.59E+15	0.140	5.84E+05	5.38E+05	1.1	5.02E+17
0.002	4.80E-02	5.88E-05	815.5	7.18E+15	0.150	6.73E+05	6.25E+05	1.1	5.38E+17
0.003	2.87E-01	3.23E-03	88.9	1.08E+16	0.160	7.67E+05	7.15E+05	1.1	5.74E+17
0.004	1.15E+00	3.99E-02	28.8	1.44E+16	0.180	9.65E+05	9.08E+05	1.1	6.46E+17
0.005	3.44E+00	2.36E-01	14.6	1.79E+16	0.200	1.18E+06	1.11E+06	1.1	7.18E+17
0.006	8.44E+00	9.09E-01	9.3	2.15E+16	0.250	1.74E+06	1.67E+06	1.0	8.97E+17
0.007	1.79E+01	2.66E+00	6.7	2.51E+16	0.300	2.35E+06	2.27E+06	1.0	1.08E+18
0.008	3.39E+01	6.43E+00	5.3	2.87E+16	0.350	2.99E+06	2.90E+06	1.0	1.26E+18
0.009	5.90E+01	1.35E+01	4.4	3.23E+16	0.400	3.64E+06	3.55E+06	1.0	1.44E+18
0.010	9.62E+01	2.56E+01	3.8	3.59E+16	0.450	4.30E+06	4.21E+06	1.0	1.61E+18
0.011	1.48E+02	4.47E+01	3.3	3.95E+16	0.500	4.96E+06	4.87E+06	1.0	1.79E+18
0.012	2.19E+02	7.31E+01	3.0	4.31E+16	0.600	6.28E+06	6.18E+06	1.0	2.15E+18
0.013	3.11E+02	1.13E+02	2.7	4.67E+16	0.700	7.58E+06	7.49E+06	1.0	2.51E+18
0.014	4.29E+02	1.68E+02	2.5	5.02E+16	0.800	8.86E+06	8.77E+06	1.0	2.87E+18
0.015	5.75E+02	2.40E+02	2.4	5.38E+16	0.900	1.01E+07	1.00E+07	1.0	3.23E+18
0.016	7.53E+02	3.33E+02	2.3	5.74E+16	1.000	1.13E+07	1.13E+07	1.0	3.59E+18
0.018	1.22E+03	5.93E+02	2.1	6.46E+16	1.250	1.43E+07	1.42E+07	1.0	4.49E+18
0.020	1.85E+03	9.71E+02	1.9	7.18E+16	1.500	1.71E+07	1.70E+07	1.0	5.38E+18
0.025	4.34E+03	2.60E+03	1.7	8.97E+16	1.750	1.97E+07	1.97E+07	1.0	6.28E+18
0.030	8.36E+03	5.47E+03	1.5	1.08E+17	2.000	2.22E+07	2.22E+07	1.0	7.18E+18
0.040	2.19E+04	1.60E+04	1.4	1.44E+17	2.500	2.69E+07	2.68E+07	1.0	8.97E+18
0.050	4.37E+04	3.42E+04	1.3	1.79E+17	3.000	3.12E+07	3.11E+07	1.0	1.08E+19
0.060	7.42E+04	6.05E+04	1.2	2.15E+17	3.500	3.51E+07	3.50E+07	1.0	1.26E+19
0.070	1.13E+05	9.51E+04	1.2	2.51E+17	4.000	3.87E+07	3.87E+07	1.0	1.44E+19
0.080	1.60E+05	1.38E+05	1.2	2.87E+17	5.000	4.53E+07	4.52E+07	1.0	1.79E+19
0.090	2.15E+05	1.88E+05	1.1	3.23E+17	6.000	5.10E+07	5.10E+07	1.0	2.15E+19
0.100	2.77E+05	2.46E+05	1.1	3.59E+17	7.000	5.60E+07	5.60E+07	1.0	2.51E+19
0.110	3.45E+05	3.10E+05	1.1	3.95E+17	8.000	6.05E+07	6.04E+07	1.0	2.87E+19
0.120	4.19E+05	3.81E+05	1.1	4.31E+17	9.000	6.44E+07	6.44E+07	1.0	3.23E+19
0.130	4.99E+05	4.57E+05	1.1	4.67E+17	10.000	6.79E+07	6.79E+07	1.0	3.59E+19